Center for Nondestructive Evaluation Publications   Center for Nondestructive Evaluation

5-1996

Elastic wave scattering by shelled spherical scatterers in a focused field

John Mittleman
United States Navy

R. Bruce Thompson
Iowa State University

Y. K. Han
Iowa State University

Follow this and additional works at: http://lib.dr.iastate.edu/cnde_pubs

Part of the Materials Science and Engineering Commons, and the Structures and Materials Commons

The complete bibliographic information for this item can be found at http://lib.dr.iastate.edu/cnde_pubs/10. For information on how to cite this item, please visit http://lib.dr.iastate.edu/howtocite.html.

Elastic wave scattering by shelled spherical scatterers in a focused field

Abstract

Embrittlement of many important metal alloys has been related to the accumulation of undesirable materials at grain boundaries, a condition which may be detectable through measurement of ultrasonic scattering from the material's microstructure. Grains with decorated grain boundaries are modeled as shelled microspheres embedded in an isotropic elastic host, and a practical means of predicting scattering from these particles is developed. The incident field often used for measuring backscattered grain noise is focused; both plane and focused incident fields are treated. Theoretical predictions of scattering from isolated scatterers are compared with experimental measurements on metal microspheres embedded in plastic to validate the computational procedure, then predictions of scattering from similar spherical structures embedded in a metal host are presented. In the former case theoretical predictions are found consistent with observations, although differences between shelled and nonshelled scatterers are obscured by the great contrast between host and scatterer. In the latter case, where host and core are quite similar, even thin shells can produce scattering readily distinguishable from the weak scattering in polycrystals that may be due to locally inhomogeneous properties. Results of this study can be used to calculate a backscattering coefficient for calculations of grain noise in metals containing, or composed of, numerous shelled scatterers.

Keywords

elastic waves, embrittlement, alloys, metals, grain boundaries, microstructure, acoustic measurements, ultrasonic waves, scattering, spheres, composite materials

Disciplines

Aerospace Engineering | Materials Science and Engineering | Structures and Materials

Elastic wave scattering by shelled spherical scatterers in a focused field

John Mittleman
Naval Surface Warfare Center, Dahlgren Division, Coastal Systems Station, Panama City, Florida 32407

R. B. Thompson and Y. K. Han
Center for Nondestructive Evaluation, Iowa State University, Ames, Iowa 50011

Embrittlement of many important metal alloys has been related to the accumulation of undesirable materials at grain boundaries, a condition which may be detectable through measurement of ultrasonic scattering from the material's microstructure. Grains with decorated grain boundaries are modeled as shelled microspheres embedded in an isotropic elastic host, and a practical means of predicting scattering from these particles is developed. The incident field often used for measuring backscattered grain noise is focused; both plane and focused incident fields are treated. Theoretical predictions of scattering from isolated scatterers are compared with experimental measurements on metal microspheres embedded in plastic to validate the computational procedure, then predictions of scattering from similar spherical structures embedded in a metal host are presented. In the former case theoretical predictions are found consistent with observations, although differences between shelled and nonshelled scatterers are obscured by the great contrast between host and scatterer. In the latter case, where host and core are quite similar, even thin shells can produce scattering readily distinguishable from the weak scattering in polycrystals that may be due to locally inhomogeneous properties. Results of this study can be used to calculate a backscattering coefficient for calculations of grain noise in metals containing, or composed of, numerous shelled scatterers. © *1996 Acoustical Society of America.*

PACS numbers: 43.35.Cg, 43.35.Zc, 43.35.Bf, 43.20.Gp

INTRODUCTION

Interface and grain boundary conditions in composite and metal materials are critically important to the macroscopic engineering properties of these materials. For example, the presence of nitrogen and oxygen in the titanium alloy, titanium–6 aluminum–4 vanadium (Ti64) leads to stabilization of the brittle ''hard alpha'' phase in Ti64, and an increased risk of crack initiation at such sites. As a step toward developing ultrasonic techniques to characterize such structures, our prior studies modeled a metal grain with foreign materials accumulated on its boundaries as a shelled spherical structure, and predicted scattering of a plane longitudinal elastic wave from such a scatterer.[1] In this paper we extend our models to predict elastic wave scattering from shelled, spherical scatterers in a focused ultrasonic beam, motivated by the practical problem of including in scattering calculations a titanium nitride (TiN) coating on particles of Ti64. The results of confirming experiments are also reported.

Scatterers adopted for experiments in the present study were microspheres produced in the course of studies on the detectability of hard alpha inclusions in Ti64.[2] These microspheres resemble the model structure extremely well, and it was possible to embed individual microspheres in plastic for a convenient and direct comparison of theory with experiment. Samples compacted from these microspheres by the hot isostatic press (HIP) procedure were also available, and serve to model a material with an accumulation of second phase materials at grain boundaries. In a separate paper we will use an independent scatterer model[3] to predict grain noise in the compacted materials from properties of the individual scattering regions.

This paper is organized as follows: in Sec. I we discuss the relationship of this work with prior studies; in Sec. II we present equations for scattering from layered spherical obstacles, and convenient representations for plane and focused fields; in Sec. III we validate computational procedures by direct comparison of computed and observed echoes, and then present results of computations wherein scatterer size and shell thickness are systematically varied. In Sec. IV we present details of the experiments and results of measurements on 217 microspheres; these results are compared with predictions from the previous section in Sec. V. Section VI presents a summary and conclusions.

I. BACKGROUND

Analytic solutions for ultrasonic wave scattering by isolated isotropic spherical obstacles in a plane, longitudinal ultrasonic field were introduced by Faran[4] for solid obstacles in a liquid host, and by Ying and Truell[5] for solid obstacles in an isotropic elastic host. These solutions, which now appear in standard texts,[6–8] rely on a convenient decomposition into longitudinal and shear waves, and on separation of equations in the radial and angular variables. More complicated problems of practical interest include layered and anisotropic scatterers,[1,9–11] scatterers of arbitrary shape,[12,13] and scatterers in a focused beam.[14] In general it is necessary to approach these problems by invoking simplifying assumptions

or by resorting to numerical methods of solution (e.g., approximate interface properties,[15–17] discretized shapes,[18] boundary and finite element methods).[12,13,19,20]

Ueda *et al.*[14] extended Faran's work on scattering from an elastic sphere in a fluid medium, expressing the field due to an incident spherical wave in terms of spherical harmonics, with the origin at the center of the scatterer rather than at the center of the source. This is then extended to the fields of focused transducers by integration of elementary spherical sources over the surface of a curved transducer. Both transmitting and receiving transducers are considered, and results for scatterers at or near the focal point are given. Bennink[21] presents a rigorous derivation of spherical wave expansion coefficients for scattering from an elastic sphere, and applies these results to the inverse problem of characterizing and immersion transducer from experimental measurements.

Roberts[22] solved for the transmission of a focused Gaussian beam through an elastic host containing an elastic sphere, extending the Ying and Truell solution not only in the form of the beam, but also by allowing for attenuation through complex wave numbers. This solution generates coefficients for an expansion of the incident focused Gaussian beam in terms of spherical harmonics, and calculates coefficients of the scattered wave (also in terms of spherical harmonics) by imposing boundary conditions at the surface of the spherical scatterer. Numerical integration of the Hankel transform of the incident beam potential in one plane is required, and evanescent waves are ignored.

Boström and Wirdelius[23] have studied an additional aspect of the problem by calculating the field of an unfocused, but finite-sized transducer used as transmitter and receiver for ultrasonic inspection. In their approach the scatterer's response is represented by a T matrix which, for a spherical scatterer, can be calculated by the separation of variables method used in the present study. Their illuminating field is represented as a plane-wave expansion which is transformed to spherical waves centered at the scatterer. Auld's reciprocity relationship[24] is used to determine the transducer's electrical output in terms of the T matrix and coefficients of the spherical wave expansion. In principle, this approach allows scatterers to be located at positions other than the transducer's focal point.

Our present work extends these previous studies by providing a general method of generating expansion coefficients for the incident field, suitable for a separation of variables solution. Any of the literature's exact and approximate expression for beam potential can be applied by creating a generalized Fourier series representation in which Legendre polynomials form the basis set. Numerical integration of these basis functions times the displacement potential and its derivative with respect to radius is required only at radii where boundary conditions will be applied.

II. THEORY

A. Incident plane wave

Ying and Truell studied scattering by spherical obstacles in an isotropic elastic solid, relying on a Helmholtz decomposition of waves with symmetry about an axis through the center of the obstacle and in the direction of propagation of the incident plane, harmonic, longitudinal wave:[5]

$$\bar{u} = -\bar{\nabla}\Psi + \bar{\nabla}\times\{\bar{\nabla}\times(\bar{r}\,\Pi)\}, \tag{1}$$

where $\bar{u}$ is the displacement vector, and Ψ and Π satisfy:

$$(\nabla^2+k^2)\Psi=0 \quad \text{and} \quad (\nabla^2+\kappa^2)\Pi=0 \tag{2}$$

with k and κ being the longitudinal and transverse wave propagation constants, respectively.

Solutions to these equations are given in terms of spherical harmonics:

$$\Psi = \sum_{m=0}^{\infty} L_m f_m(kr) P_m(\cos\theta)$$

and

$$(3)$$

$$\Pi = \sum_{m=0}^{\infty} T_m f_m(\kappa r) P_m(\cos\theta)$$

in which radial and angular dependencies are separated. Assuming the time dependence to be $e^{i\omega t}$, the terms $f_m()$ are spherical Hankel functions of the second kind for the outward propagating scattered field, and spherical Bessel functions for the incident field and the field inside the scatterer. The coefficients L_m and T_m define longitudinal and transverse waves, respectively, and are found by balancing stresses and displacements for each order, m, at each interface.

This method of solution is easily applied to layered spherical obstacles in what can be considered an "extended" Ying and Truell solution.[25] Four equations (continuity of normal and tangential displacements and stresses, given explicitly in the Appendix) are required at each interface. Because continuity at each interface depends on the fields in the two regions adjacent to that interface, only, the matrix of continuity equations is block diagonal, and susceptible to efficient numerical algorithms.[26] Solutions in each layer are written as a combination of inward and outward traveling waves (spherical Hankel functions of the first and second kind), or equivalently, as a combination of spherical Bessel and Neumann functions.

Schmidt[27] has noted numerical instabilities that are inherent in the choice of spherical Hankel functions as the independent set of basis functions used to describe the scattered field. While this set enjoys a straightforward physical interpretation and is theoretically independent, it becomes dependent, numerically, at high order. This can be seen by noting that for high order, and argument less than order, the real part of the Hankel functions becomes insignificant with respect to the imaginary part;[6,28] $h_n^{1,2}(kr) \rightarrow \pm i y_n(kr) \rightarrow \pm i\infty$ for $n\rightarrow\infty$. This becomes a computational problem because small differences between the inward and outward traveling waves in the shell must be computed properly in order to match boundary conditions. We overcome this problem by choosing the independent set of spherical Bessel functions, $j_n(kr)$ and $y_n(kr)$ instead of the Hankel functions, $h_n^1(kr)$ and $h_n^2(kr)$ and by ordering the equations to ensure that evanescent components which are physically uncoupled are also numerically uncoupled. The
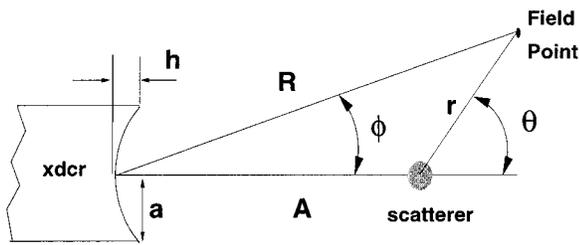
FIG. 1. Geometry of a focused transducer.

effect of this maneuver is to form the required differences between coefficients before multiplying them by the very large imaginary, or very small real parts of the Hankel functions.

B. Incident focused fields

The plane-wave assumption which is often invoked in analytical scattering calculations allows the incident wave to be written in many ways, where the geometry and position of the scatterer will dictate the choice of basis functions (e.g., plane, cylindrical, or spherical). For the present studies, where the scattered field is expanded in spherical harmonics,[5] it would be convenient to express an arbitrary incident field as the sum of some function of radius and order only, multiplied by the Legendre polynomial of the appropriate order.

H. T. O'Neil[29] analyzed radiation into a fluid from a transducer with a spherical concave piezoelectric element, starting from the Rayleigh integral, and gives an approximate expression for the field's velocity potential near the focal plane. For geometries that satisfy O'Neil's assumptions that wavelength and the depth of the concave surface are both much less than the transducer element's radius, this expression (integrated once with respect to time to obtain a displacement potential) is appropriate for analysis of scattering from a small obstacle at, or near the focus of the transducer:

$$\Psi \approx \left(\frac{1}{i\omega}\right)(vS)\frac{e^{-ikR}}{2\pi R}\left(\frac{2}{z}\right)J_1(z), \tag{4}$$

where (vS) represents the surface velocity times surface area of the transducer element, R is the distance from the center of the transducer's surface to the field point (in the vicinity of the transducer's focus) and $z=(1-i/kR)ka\sin\phi \approx ka\sin\phi$ (as shown in Fig. 1, a is the transducer element's radius, and ϕ is measured from the transducer axis to the field point, with the vertex of the angle on the face of the transducer).[30]

While O'Neil's expression was derived for the acoustic case we will be using it extend the field across a liquid/solid interface to calculate scattering in an isotropic solid medium. Numerous studies of propagation across liquid/solid interfaces have been undertaken, owing to the practical importance of immersion testing, and excellent results have been demonstrated for theories based on the Fresnel, or paraxial, approximation.[31–33] When dealing with paraxial rays normally incident on the interface, these studies have shown that the field in the solid propagates as a version of the field that

would exist in the fluid, scaled in the direction of propagation by the ratio of longitudinal wavespeeds and by the inverse of this ratio across the beam. One significant result of this is that although the focal point is shallower in the solid than it would have been in the fluid, the beamwidth in the transducer's focal plane is unaltered by the medium in which the focal point occurs. When comparing focus in water to focus in the solid under these conditions, field strength at the focal point need only be modified by the transmission coefficient and a phase factor.[31] In the present case, where the angle subtended by the scatterer in the transducer's field of view is small, and our interest is in the field in the vicinity of the focal point, the paraxial approximation is justified. For a pulse excitation, shear waves that may be produced at the interface are neglected, as they will be separated in time from the longitudinal waves.

Although the expression for Ψ in Eq. (4) is not given in terms of spherical harmonics, a generalized Fourier series representation[34] is possible, wherein the basis comprises the Legendre polynomials. Recalling that the Legendre polynomials form a complete, orthogonal set over the interval $(-1,1)$ with respect to a constant weighting function, and since O'Neil's approximate expression is continuous and square integrable on that interval, we may write:

$$\Psi = \sum_{m=0}^{\infty} a_m(r)P_m(\cos\theta), \tag{5}$$

with

$$a_m(r) = \int_{-1}^{1} \Psi(r,x)P_m(x)dx, \tag{6}$$

where $x=\cos\theta$, r is measured from the transducer's focal point to the field point, and θ is measured from the transducer's axis to the field point, with the vertex of the angle at the transducer's focal point. From Fig. 1 we note that r and θ are related to R and ϕ by the following: $R\sin\phi=r\sin\theta$ and $R^2=A^2+r^2+2Ar\cos\theta$ (A is the transducer element's focal length[35]). The required integrals are efficiently evaluated using Gauss–Legendre quadrature.[28,36]

In calculating displacements and stresses at the scatterer's spherical boundaries, all derivatives with respect to θ are performed only on the term $P_m(x)$ and all derivatives with respect to r are performed only on the coefficients, $a_m(r)$, and may in fact be performed under the integral. Explicit expressions are given in the Appendix.

To complete discussion of the potential field we mention that the technique embodied by Eqs. (5) and (6) is easily implemented whenever the field and its derivative with respect to r can be calculated on the spherical boundaries. For example, should the more rigorous expression given by O'Neil, or the Gaussian potential given by Thompson and Lopes[31] be desired, the only resulting changes to numerical code will be the expressions which evaluate Ψ and $\partial\Psi/\partial r$ on the obstacle's spherical surface.

TABLE I. Properties of microspheres and host materials.

Composition	At. % nitrogen	At. % oxygen	C_L (km/s)	C_T (km/s)	Density (g/cm^3)
Titanium–6Al–4V			6.175	3.151	4.461
Titanium nitride	28.35	4.01	7.902	4.350	4.621
Plastic host			2.73	1.43	1.18
Ti64 host			6.191	3.186	4.490

C. Time domain waveform reconstruction

By solving the equations which balance displacements and stresses on the scatterer's spherical surface we arrive at the coefficients L_m and T_m required to calculate the scattered field:

$$\Psi^s = \sum_{m=0}^{\infty} L_m h_m^{(2)}(kr) P_m(\cos\theta)$$

and
$$\qquad\qquad (7)$$

$$\Pi^s = \sum_{m=0}^{\infty} T_m h_m^{(2)}(\kappa r) P_m(\cos\theta).$$

Using approximate expressions for spherical Hankel functions when the argument is large, we can calculate the equivalent of a longitudinal wave far-field scattering amplitude:

$$A^L(\theta) = \sum_{m=0}^{\infty} -L_m e^{im(\pi/2)} P_m(\cos\theta), \qquad (8)$$

where $A^L(\theta)$ is defined by the equation:

$$u_r^s(r,\theta,\omega) \approx A^L(\theta) \left\{ u^0(\omega)\frac{e^{-ikr}}{r} \right\} \qquad (9)$$

in which u^0 is the magnitude of the incident field at the center of the scatterer and accounts for initial field strength, transmission through the interface, and travel in the solid.

From Eq. (9) one can associate scattering amplitude with the Fourier transform of an impulse response for the scatterer, for which the magnitude of the incident field would be unity at all frequencies. To compute the response of the scatterer that would be observed with a measurement system of finite beamwidth, this impulse response must be convolved with the shape of a reference pulse which characterizes the system's response. Here, we have inferred that shape from an interface echo experimentally recorded. More specifically, scattering amplitude, computed at evenly spaced values of ka (based on the longitudinal wave velocity in the host, and the obstacle's outer radius), is considered to be the discrete Fourier transform (DFT) for positive frequencies; the complete DFT is constructed by adding a symmetric real extension and an antisymmetric imaginary extension. It should be noted that in order to properly match the point-by-point multiplication of this sequence with the DFT of a reference interface echo, scattering amplitudes must be calculated for values of ka from zero to $(\pi a)/(\tau c_L)$ where τ is the sampling interval for the reference echo, and the number of values of ka calculated is half the number of samples in the reference echo waveform.

III. NUMERICAL STUDIES

Implementing the procedures discussed above in a fashion which avoided numerical instability resulted in code which was stable up to values of ka well over 100. To validate our time domain reconstruction method, a microsphere 0.292 mm in diameter (composed of a Ti64 core 0.266 mm in diameter with a nitrided shell estimated to be 6 to 8 μm thick), embedded in plastic, was studied both experimentally and by calculating its predicted response. Physical properties of these materials are given in Table I. The incident field was taken to be that of a 12.7-mm focal length transducer with a concave piezoelectric element having a 5.84-mm radius (these dimensions were chosen to match the field of the transducer used for experiments). The equivalent scattering amplitude was calculated in accordance with the theory outlined for focused incident fields, and the representative interface echo was obtained directly by placing the transducer above a plane interface at the transducer's focal position. Calculated and measured responses were aligned in time and scaled such that the direct reflections match; these are shown in Fig. 2(a)–2(b). Early portions of the calculated response are expected to correspond closely to experimental measurements by virtue of the alignment and scaling, but later portions of the response (which are thought to be due to propagation along the plastic/metal interface) also show excellent agreement. In Fig. 2(c) we show that the use of a plane incident field results in significant errors, which is not surprising since the diameter of the scatterer exceeds the 6-dB beamwidth in the focal plane.

Variations in shell thickness, with all other parameters held constant, lead to noticeable differences in both the amplitude and arrival time of the second peak in the computed waveform. Figure 3(a) shows time delay between peaks derived from the envelopes of waveforms computed for a scatterer having an outside diameter of 0.292 mm and a shell of variable thickness. This delay time diminishes monotonically with increasing shell thickness, and corresponds very roughly to circumnavigation of the scatterer by a wave traveling at 3.33 mm/μs when shell thickness is zero and 4.70 mm/μS when the shell is 110 μm thick.[37] We think that these are surface waves, since refraction at the host/microsphere interface favors their generation. That their apparent phase velocities are slightly higher than the corresponding Rayleigh wave velocities (approximately 2.96 mm/μs for Ti64 and 4.02 mm/μs for TiN) may be due to the curvature of the surface on which they are traveling. Viktorov[38] presents a theoretical solution for surface waves circumnavigating a cylindrical surface, and shows that phase velocity is a function of the curvature-to-wavelength ratio,
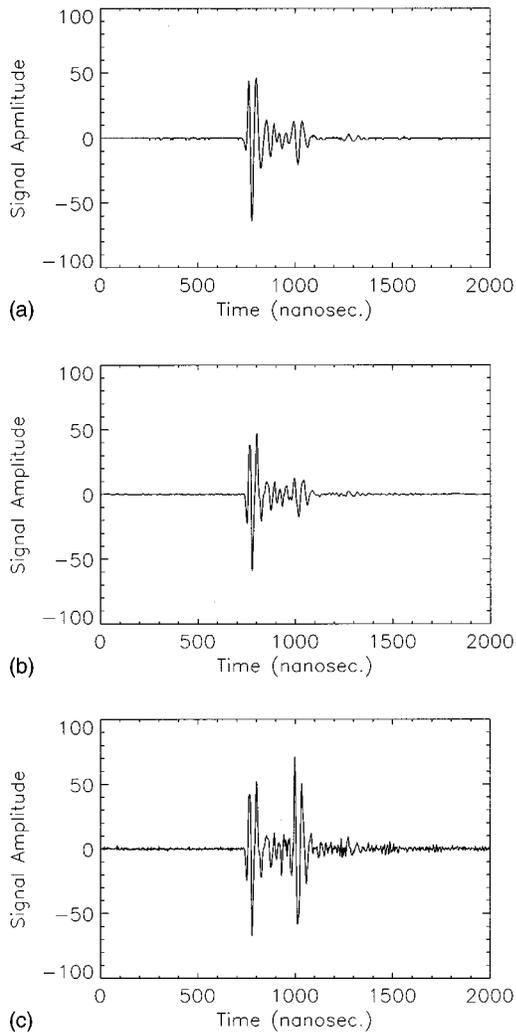
FIG. 2. (a) Measured signal from a 0.292-mm nitrided microsphere using a 50-mHz focused transducer. (b) Calculated signal for a 0.292-mm nitrided microsphere using a 50-mHz focused transducer. (c) Calculated signal for a 0.292-mm nitrided microsphere using a 50-mHz flat transducer.
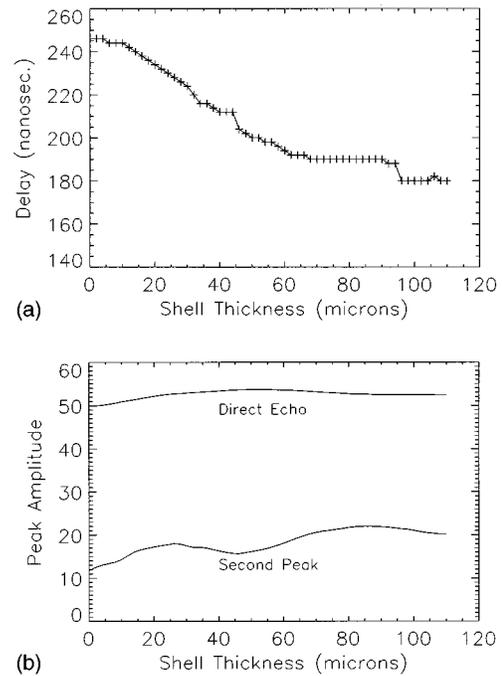

FIG. 3. (a) Effect of varying shell thickness on the time delay between the direct and second waveform peaks. (b) Effect of varying shell thickness on amplitude of the direct and second waveform peaks.

and is slightly larger than the Rayleigh velocity. From his work we estimate the ratio of phase velocity to Rayleigh wave speed to be approximately 1.2, for the conditions under which our time domain reconstructions were performed.

Figure 3(b) shows the amplitude of the second peak of the waveform envelopes described above. There appears to be a significant dependance on shell thickness, with interferencelike variations that have not been completely investigated. By comparison, the amplitude of the first peak was relatively unaffected, as would be indicated by a calculation of the coefficient of reflection at normal incidence for Ti64 or TiN in plastic (values for the coefficient of reflection are 0.79 and 0.84, respectively).

Varying scatterer size while holding shell thickness constant approximates the experimental situation described in the next section. In order to limit the maximum value of ka required for time domain reconstructions, calculations for microspheres with an outer radius from 0.075 to 0.175 mm were carried out with 2-ns point spacing. Time domain reconstructions were performed for Ti64 scatterers with no shell, and with a shell 0.0065 mm thick. These calculations

predicted that it would be difficult to experimentally observe the small difference between scatterers with and without a shell, embedded in plastic with an acoustic impedance far less than that of the scatterers in either condition. In the practical case of scatterers in a more similar host (e.g., a grain of metal with decorated boundaries embedded in an otherwise homogeneous metal host) we expect the effect of shell composition and thickness to be more readily observed. In Fig. 4(a) we show the calculated response of a Ti64 microsphere embedded in a host with similar, but not identical properties. Material constants for the core are those given by Gigliotti *et al.*[39] for Ti64, while those for the host are based on measurements on a solid sample compacted from Ti64 powder;[40] values are given in Table I. By comparison to the same scatterer embedded in plastic [see Fig. 2(b)], these results show the circumnavigating wave's arrival considerably earlier, consistent with the host's higher velocities. The amplitude of the scattered signal is diminished by approximately two orders of magnitude, reflecting the host and scatterer's similar acoustic impedances. In Fig. 4(b) we show that the signal scattered from a nitrided microsphere in the Ti64 host is significantly greater than that scattered by the unshelled Ti64 microsphere, despite the fact that shell thickness is far less than one wavelength thick. The rich structure of the nitrided sphere's response suggests a dispersive process in the layered microsphere. These results are suitable input for scattering predictions of grain noise based on the independent scattering model.[3,41,42]

IV. EXPERIMENTAL STUDIES

With a long range view to predicting ultrasonic scattering in materials containing, or composed of, scatterers mod-
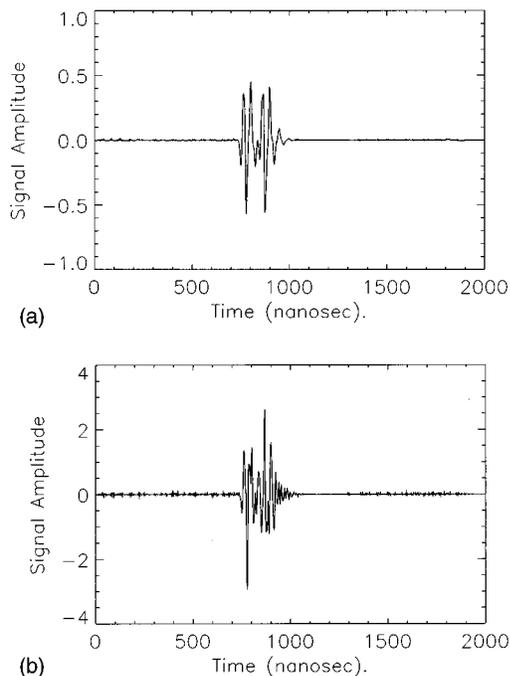
FIG. 4. (a) Calculated scattered signal for a 0.292-mm-diam Ti64 microsphere in a host similar to Ti64, inspected with a focused 50-mHz transducer. (b) Calculated scattered signal for a 0.292-mm-diam nitrided Ti64 microsphere in a Ti64 host, inspected with a focused 50-mHz transducer.

FIG. 5. Scanning electron microscope image of consolidated material formed from nitrided Ti64 microspheres.

eled by the shelled spheres described above, the validity of our models for the illuminating fields and for the signal backscattered from isolated scatterers was tested by comparing predictions with experimental observations. The theoretical work dealt with a shelled spherical scatterer in an isotropic host, inspected ultrasonically with a focused beam. In our experiments the shelled scatterers were Ti64 microspheres on which a nitrided outer layer had been produced, the host was metallurgical mounting plastic, and the focused beam was produced by the inspection system described below.

A. Properties of the microspheres

Our experiments were conducted on samples of Ti64 microspheres and nitrided Ti64 microspheres. The Ti64 microspheres were prepared as they would be for commercial powder metallurgy applications by Nuclear Metals, Inc., Concord, MA. Chemical analysis of the Ti64 material, in its powder state, showed the aluminum content to be 6.45 wt %, vanadium 4.20 wt %, nitrogen 0.009 wt %, and oxygen 0.186 wt %. A portion of the Ti64 powder was heated in a nitrogen atmosphere at 1000 °C for 24 h to produce a shell of TiN_x. Composition of the shell was estimated from x-ray diffraction results to be approximately 30 at. % nitrogen.

In calculating the theoretical response for shelled microsphere we have used velocities and density corresponding to values measured by Gigliotti et al.[39] for a sample 28.35 at. % nitrogen (similar to the XRD estimate of 30 at. %) and 4.01 at. % oxygen (approximately 1.73 wt % oxygen). Values for density and wavespeeds corresponding to the two compositions are shown in Table I.
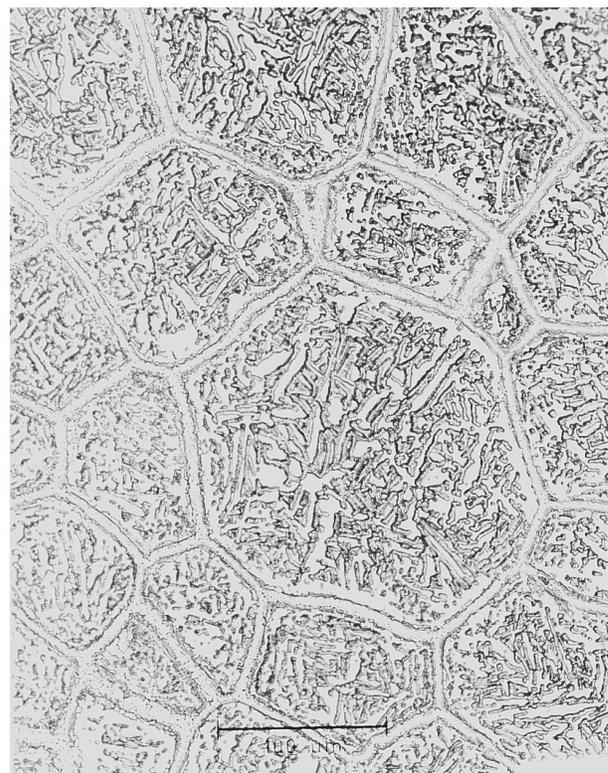
SEM images of consolidated nitrided microparticles, Fig. 5, suggest that the thickness of the shell is roughly as 6 to 8 μm, independent of particle diameter; the importance of shell thickness on scattering amplitude, or equivalently, impulse response, has already been discussed. This estimate of shell thickness is reasonably well supported by independent x-ray diffraction results, from which we have estimated the volume percent TiN_x to be 19.7% where particles in the powder sample measured ranged from under 100 μm to over 400 μm in diameter. Optical measurement of 140 microparticles gives a volume-averaged mean diameter of 249 μm; a shell 8.8 μm thick on the mean particle would constitute 19.7% of the volume.

B. Experimental samples

Two sets of microspheres were mounted in plastic to facilitate ultrasonic and optical measurements. One set of microspheres was Ti64 in its original condition, and the other set was nitrided Ti64 microspheres. Buehler Transoptic Powder #20-3400-080 was first formed into a disc somewhat less than the final specimen thickness by melting the powder at 320°±5 °F (160°±2 °C) and 4200 psi (28.95 MPa) in a Leco PR-22 Pneumatic mounting press. A 0.1-in.-square grid was established on this lower-mold-half by indenting the plastic with a scribe. A section of graph paper was used as a template to position the indentations on a grid consisting of 117 sites, arranged in 11 rows and columns, minus the 4 corners. Individual microparticles were then picked up with a plastic tool to which the particles adhered electrostatically, and deposited in the prepared sites. Once loaded with micro-
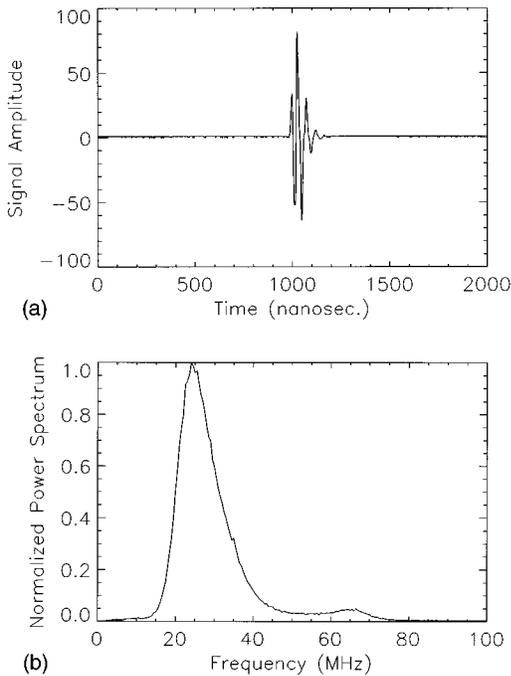
FIG. 6. (a) Interface echo produced by a 50-mHz focused transducer. (b) Power spectrum of the interface signal.

spheres, the lower-mold-half was carefully reinserted into the mounting press and covered with Transoptic powder to form the upper-mold-half. These materials were then reprocessed to form the final molded specimens, 1.5 in. (38.1 mm) in diameter, 0.57 in. (14.5 mm) thick, with the microspheres arranged on a plane 0.1 in. (2.5 mm) below the top surface.

C. Ultrasonic inspection system

The ultrasonic inspection system consisted of a Panametrics Model UA5600 pulser/receiver, a focused 50-mHz immersion transducer (described below), and a Tektronix 7603 oscilloscope with a 7D20 programmable digitizer. Waveform information was transferred through a Metrabyte IEEE-488 board (MBC-488) to a Compaq Portable 386-20 computer (model 2670) for acquisition and processing. To achieve maximum sensitivity, the pulser/receiver was set to maximum energy output with minimum attenuation and damping.

The 50-mHz ultrasonic transducers used were Panametrics models V390 and V3884, both of which are focused at 0.5 in. (12.7 mm) by means of a lens ground in the face of the buffer rod. The principal difference between these two transducers is that the buffer rod diameter on the V3884 is twice as large as the V390, resulting in a significant reduction in internal echoes and artifacts. We found that the apparent center frequency is shifted downward by transmission through water, and that in the vicinity of the geometric focal point the field, and its spectrum, change rapidly. From Fig. 6(a) and (b), which show a typical echo from a plane surface at the geometric focal position of the V3884 transducer, and the corresponding spectrum, we note that the peak frequency is considerably less than 50 mHz; this departure from nominal performance was also evident in all of the measured

waveforms. Using the echo shown in Fig. 6(a) as a reference for time domain reconstructions captures the essential features of the transducer and propagation through water, but neglects frequency dependent attenuation in the mounting plastic as well as the effects of diffraction on the reference waveform.

Based on O'Neil's approximate expression for the field of a spherically focused transducer, one estimates the 6-dB beamwidth (in the focal plane) to be

$$1.03 \, \frac{\lambda A}{d}, \tag{10}$$

where λ is wavelength, A is the transducer's radius of curvature and d is the element's diameter. Substituting focal length in water for the element's radius of curvature, we take this expression (derived for a spherically concave piezoelectric element) as an approximate expression for the transducers we used, which focus by means of a spherically ground lens in the buffer rod. Using this expression for the V390 transducer, for which the center frequency of an interface echo is approximately 25 mHz, we find a theoretical value of 122 μm for the 6-dB beamwidth. Direct measurement of the beamwidth is hindered by difficulties in finding a target much smaller than the beamwidth; even the smallest of the targets mounted in Transoptic plastic is larger than the calculated beamwidth. Beamwidth measurements on ten microspheres ranging from 170 to 391 μm in diameter produced an average ($\pm$standard deviation) beamwidth of 96.2$\pm$8.1 μm.

D. Data acquisition

The signal from each microsphere was peaked up using manual micrometer and goniometer adjustments while observing the oscilloscope screen, and arrival time was checked to ensure that the depth of the microsphere was in the focal region of the transducer. After carefully positioning the transducer over each of the microspheres, the signal was averaged over 16 returns (to reduce electrical noise) and captured as a 1024-point waveform. As each waveform was acquired, digital cursors were used to measure the time delay from the direct return to the circumnavigating wave return.

V. COMPARISON WITH THEORY

From the ultrasonic waveforms and optical measurements of each microsphere we are able to plot time delay (between the major negative spikes in the interface echo and the ''circumnavigating wave'' return) against microparticle diameter. Predicted values for this relationship are also available from the waveform reconstructions discussed above, and indeed, a small difference between the diameter-to-delay ratios for shelled and nonshelled particles was observed experimentally and in theory. Figure 7 shows good agreement between measurements on 217 microspheres and values derived from waveform reconstructions. For the experimental data set obtained with the V390 transducer, the average diameter/delay ratio ($\pm$standard deviation) was 1.217$\pm$0.041 mm/μS for the Ti64 microspheres and 1.256$\pm$0.086 mm/μS for the TiN microspheres. These values can be compared

2868   J. Acoust. Soc. Am., Vol. 99, No. 5, May 1996
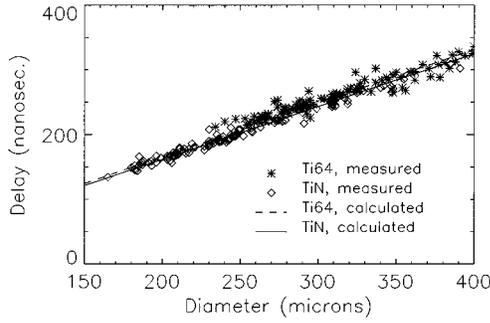
Mittleman *et al.*: Elastic wave scattering   2868

FIG. 7. Delay time versus diameter for shelled and nonshelled microspheres.

with those based on waveform reconstructions; 1.201 ± 0.007 for Ti64, $1.210\pm.0134$ for microspheres with a 6.5 μm TiN shell, or $1.236\pm.004$ for microspheres with a 13-μm TiN shell. (Variance in the values based on waveform reconstruction are due in part to discretization and in part to interference of waveform features for very small diameters.) In the presence of the experimental error noted above, these data fail to clearly indicate the presence, or absence of a nitride shell when the scatterer is embedded in a host quite different from the scatterer. However, the basic computational method appears to predict scattering well enough in this case to adopt it for studies of scattering when the host and scatterer are quite similar.

VI. SUMMARY AND CONCLUSIONS

Elastic scattering of a focused ultrasonic field by shelled spherical obstacles was studied as a first step in predicting scattering from materials composed of polycrystals that may have abnormal grain boundary structures. Good agreement was obtained when calculated and experimental results were compared.

Theoretical calculations were based on a separation of variables method which represents the incident and scattered fields as series for which the basis functions are Legendre polynomials. Coefficients for the incident field were calculated by representing an approximate expression for the field as a generalized Fourier series using Legendre polynomials as the orthogonal basis set. This allowed direct use of code previously developed for calculating scattering from shelled spherical obstacles in a plane wave field.[25]

Numerical stability problems associated with properly combining inward and outward propagating partial waves in the shell were addressed by choosing numerically independent functions of radius (spherical Bessel and Neumann functions) rather than the more commonly used spherical Hankel functions. Our calculations were stable over a wide range of obstacle sizes and shell thickness, up to a wave number sufficient for inversion of frequency domain results into the time domain.

A complex scattering amplitude, in the backscattered direction, was calculated for a wide range of scatterers. From this, a discrete Fourier transform associated with the impulse response of the scatterer in a focused field was constructed. Multiplying this sequence by the DFT of a reference echo

and inverting the transform gave time domain waveforms directly comparable with experimentally obtained waveforms.

The generally good agreement of calculated and experimentally observed waveforms suggests that our scattering amplitude calculations are reasonably accurate. These calculations will serve as input for predictions of scattering from large numbers of independent scatterers; experimental and theoretical aspects of this work will be reported in the near future.

APPENDIX

$$u_r = -\frac{\partial\Psi}{\partial r} = -\sum_0^\infty a_{m,r}(r)P_m(x), \tag{A1}$$

$$u_\theta = -\frac{1}{r}\frac{\partial\Psi}{\partial\theta} = -\frac{1}{r}\sum_{m=0}^\infty a_m(r)P_{m,\theta}(x), \tag{A2}$$

$$\sigma_{rr} = \rho\omega^2\left\{\Psi + \left(\frac{2}{\kappa^2}\right)\left(\frac{2}{r}\frac{\partial\Psi}{\partial r} + \frac{1}{r^2}\Omega\Psi\right)\right\}$$

$$= \frac{-2}{r^2}\rho c_t^2\sum_{m=0}^\infty\left\{a_m(r)\left(m(m+1)-\frac{\kappa^2 r^2}{2}\right)\right.$$

$$\left. -2ra_{m,r}(r)\right\}P_m(x), \tag{A3}$$

$$\sigma_{r\theta} = -2\frac{\rho\omega^2}{\kappa^2}\frac{\partial}{\partial\theta}\left\{\frac{1}{r}\frac{\partial\Psi}{\partial r} - \frac{1}{r^2}\Psi\right\}$$

$$= \frac{-2}{r^2}\rho c_t^2\sum_{m=0}^\infty(ra_{m,r}(r)-a_m(r))P_{m,\theta}(x), \tag{A4}$$

where

$$P_{m,\theta}(x) = \left(-\sin\theta\frac{\partial P_m(x)}{\partial x}\right), \tag{A5}$$

$$\Omega P_m(x) = \frac{1}{\sin\theta}\frac{\partial}{\partial\theta}\sin\theta\frac{\partial}{\partial\theta}P_m(x) = -m(m+1)P_m(x), \tag{A6}$$

$$a_m(r) = \int_{-1}^1\Psi(r,x)P_m(x)dx, \tag{A7}$$

$$a_{m,r}(r) = \int_{-1}^{1} \frac{\partial \Psi(r,x)}{\partial r} P_m(x)\,dx. \tag{A8}$$

[1] J. Mittleman, R. Roberts, and R. B. Thompson, ''Scattering of Longitudinal Elastic Waves from an Anisotropic Spherical Shell,'' J. Appl. Mech. **62**(1), 150–158 (1995).

[2] L. J. H. Brasche, F. Margetan, and R. B. Thompson, ''Sample Preparation Techniques and Material Property Measurements of Hard Alpha Titanium Samples,'' in *Review of Progress in Quantitative NDE (V.11B)*, edited by D. O. Thompson and D. E. Chimenti (Plenum, New York, 1992), pp. 1733–1738.

[3] J. H. Rose, ''Ultrasonic Backscatter from Microstructure,'' in *Review of Progress in Quantitative NDE (V.11B)*, edited by D. O. Thompson and D. E. Chimenti (Plenum, New York, 1992), pp. 1677–1684.

[4] J. J. Faran, Jr., ''Sound Scattering by Solid Cylinders and Spheres,'' J. Acoust. Soc. Am. **23**, 405–418 (1951).

[5] C. F. Ying and R. Truell, ''Scattering of a Plane Longitudinal Wave by a Spherical Obstacle in an Isotropically Elastic Solid,'' J. Appl. Phys. **27**, 1086–1097 (1956).

[6] P. M. Morse and H. Feshbach, *Methods of Theoretical Physics* (McGraw-Hill, New York, 1953), pp. 1462.

[7] Y. H. Pao and C. C. Mow, *Diffraction of Elastic Waves and Dynamic Stress Concentrations* (Adam Hilger/Crane Russak, London, 1973).

[8] A. H. Harker, *Elastic Waves in Solids* (Adam Hilger/British Gas plc, London, 1988).

[9] R. Paskaramoorthy, S. K. Datta, and A. H. Shah, ''Effect of Interface Layers on Scattering of Elastic Waves,'' J. Appl. Mech. **55**, 871–878 (1988).

[10] P. Olsson, S. K. Datta, and Boström, ''Elastodynamic Scattering from Inclusions Surrounded by Thin Interface Layers,'' J. Appl. Mech. **57**(3), 672–676 (1990).

[11] A. Ben-Menahem and R. L. Gibson, Jr., ''Scattering of Elastic Waves by Localized Anisotropic Inclusions,'' J. Acoust. Soc. Am. **87**, 2300–2309 (1990).

[12] P. J. Schafbuch, R. B. Thompson, and F. J. Rizzo, ''Application of the Boundary Element Method to Elastic Wave Scattering by Irregular Defects,'' J. Nondestr. Eval. **9**(2/3), 113–128 (1990).

[13] A. F. Seybert, B. Soenarko, F. J. Rizzo, and D. J. Shippy, ''An Advanced Computational Method for Radiation and Scattering of Acoustic waves in Three Dimensions,'' J. Acoust. Soc. Am. **77**, 362–368 (1985).

[14] M. Ueda and E. Morimatsu, ''Analysis of Echoes from a Sphere Which Includes the Directivity of a Transmitter an Receiver,'' J. Acoust. Soc. Am. **87**, 1903–1910 (1990).

[15] S. K. Datta, P. Olsson, and A. Boström, ''Elastodynamic Scattering from Inclusions with Thin Interface Layers,'' in *Wave Propagation in Structural Composites-AMD Vol. 90* (Am. Soc. Mech. Engr., New York, 1988), pp. 109–116.

[16] S. I. Rokhlin and Y. J. Wang, ''Equivalent Boundary Conditions for Thin Orthotropic Layer Between Two Solid Reflectors: Reflection, Refraction, and Interface Waves,'' J. Acoust. Soc. Am. **91**, 1875–1887 (1992).

[17] J-M. Baik and R. B. Thompson, ''Ultrasonic Scattering from Imperfect Interfaces: A Quasi-Static Model,'' J. Nondestr. Eval. **4**(3/4), 177–196 (1984).

[18] P. J. Schafbuch, R. B. Thompson, F. J. Rizzo, and T. J. Rudolphi, ''Elastic Wave Scattering by Arbitrarily Shaped Voids,'' in *Review of Progress in Quantitative NDE (V.8A)*, edited by D. O. Thompson and D. E. Chimenti (Plenum, New York, 1989), pp. 15–22.

[19] L. J. Bond, ''Numerical Techniques and Their Use to Study Wave Propagation and Scattering—A Review,'' in *Elastic Waves and Ultrasonic Nondestructive Evaluation*, edited by S. K. Datta, J. D. Achenbach, and Y. S. Rajapakse (Elsevier, North-Holland, 1990), pp. 17–27.

[20] P. A. Martin, ''Boundary Integral Equations for the Scattering of Elastic Waves by Elastic Inclusions with Thin Interface Layers,'' J. Nondestructive Eval. **11**(3/4), 167–174 (1992).

[21] D. D. Bennink, ''Modelling of Ultrasonic Scattering Experiments with Applications to System and Transducer Characterization,'' Doctoral Dissertation, Dept. of Aerospace Engineering and Engineering Mechanics, Iowa State University, Ames, IA, 1990.

[22] R. A. Roberts, ''Ultrasonic NDE of Green-State Ceramics by Focused Through-Transmission,'' in *Review of Quantitative Nondestructive Evaluation, Volume 6B*, edited by D. O. Thompson and D. E. Chimenti (Plenum, New York, 1987), pp. 1443–1452.

[23] A. Boström and H. Wirdelius, ''Ultrasonic Probe Modelling and Nondestructive Crack Detection,'' Report CTH 1994:6, Division of Mechanics, Chalmers University of Technology, Göteborg, Sweden, 1994.

[24] B. A. Auld, ''General Electromechanical Reciprocity Relations Applied to the Calculation of Elastic Wave Scattering Coefficients,'' Wave Motion **1**, 3–10 (1979).

[25] J. Mittleman, R. B. Thompson, and R. Roberts, ''Ultrasonic Scattering from Anisotropic Shells,'' in *Review of Progress in Quantitative NDE (V.11)*, edited by D. O. Thompson and D. E. Chimenti (Plenum, New York, 1992), pp. 89–95.

[26] G. Strang, *Linear Algebra and Its Applications* (Harcourt Brace Javanovich, New York, 1988), 3rd ed.

[27] H. Schmidt, ''Numerically Stable Global Matrix Approach to Radiation and Scattering from Spherically Stratified Shells,'' J. Acoust. Soc. Am. **94**, 2420–2430 (1993).

[28] M. Abramowitz and I. A. Stegun, *Handbook of Mathematical Functions with Formulas, Graphs and Mathematical Tables*, National Bureau of Standards Applied Mathemmatics Series #55 (U.S. Gov't. Printing Office, 1972), 10th ed.

[29] H. T. O'Neil, ''Theory of Focusing Radiators,'' J. Acoust. Soc. Am. **21**, 516–526 (1949).

[30] O'Neil's derivation requires $kR \gg 1$, and that wavelength (λ) and the depth of the concave transducer (h) be small compared to the transducer element's radius.

[31] R. B. Thompson and E. F. Lopes, ''The Effects of Focusing and Refraction on Gaussian Ultrasonic Beams,'' J. Nondestr. Eval. **4**(2), 107–123 (1984).

[32] B. P. Newberry and R. B. Thompson, ''A Paraxial Theory for the Propagation of Ultrasonic Beams in Anisotropic Solids,'' J. Acoust. Soc. Am. **85**, 2290–2300 (1989).

[33] R. B. Thompson and T. A. Gray, ''Analytic Diffraction Corrections to Ultrasonic Scattering Measurements,'' in *Review of Progress in Quantitative Nondestructive Evaluation, Volume 2*, edited by D. O. Thompson and D. E. Chimenti (Plenum, New York, 1983), pp. 567–586.

[34] W. Magnus, F. Oberhettinger, and R. P. Soni, *Formulas and Theorems for the Special Functions of Mathematical Physics* (Springer-Verlag, New York, 1966), 3rd ed.

[35] A significant point made by O'Neil is that the focus, or point of maximum intensity, is not at the center of curvature of the transducer. O'Neil approximates the position of the focal point at $A(1 - 12/(k^2h^2 + 12))$, which approaches A for sufficiently high frequency. In our experimental work the dimensionless quantity kh was greater than 50 at the transducer's center frequency, and the resulting difference between the center of curvature and the focal point was approximately 45 μm.

[36] W. H. Press, *Numerical Recipes: The Art of Scientific Computing (FORTRAN Version)* (Cambridge U.P., New York, 1990).

[37] We note that these waves would more accurately be classified as Stonely waves, rather than Rayleigh waves, and that to speak of a ''circumnavigating wave'' is not completely appropriate since the scatterer size in these studies is sufficiently small that a ray approximation is not expected to be very accurate.

[38] I. A. Viktorov, *Rayleigh and Lamb Waves: Physical Theory and Applications* (Plenum, New York, 1967), American edition.

[39] M. F. X. Gigliotti, R. S. Gilmore, and L. C. Perocchi, ''Microstructure and Sound Velocity of Ti–N–O Synthetic Inclusions in Ti–6Al–4V,'' Metall. Mater. Trans. **25**(11), 2321–2330 (1994).

[40] Personal communication with F. J. Margetan, Iowa State University, Ames, IA.

[41] F. J. Margetan, R. B. Thompson, and I. Yalda-Mooshabad, ''Backscattered Microstructural Noise in Ultrasonic Toneburst Inspections,'' J. Nondestr. Eval. **13**(3), 111–136 (1994).

[42] I. Yalda-Mooshabad, F. J. Margetan, and R. B. Thompson, ''Monte-Carlo Simulation of Ultrasonic Grain Noise,'' in *Review of Progress in Quantitative NDE (V.12)*, edited by D. O. Thompson and D. E. Chimenti (Plenum, New York), pp. 1727–1734.